Silhouette-based 3D Model for Zebrafish High-throughput Imaging

Yuanhao Guo[1], Wouter J. Veneman[2], Herman P. Spaink[2], and Fons J. Verbeek[1]
[1] Imaging and BioInformatics Section, LIACS, Leiden University, The Netherlands
[2] Department of Animal Sciences and Health, Institute of Biology, Leiden University, The Netherlands
[1]{y.guo.3, f.j.verbeek}@liacs.leidenuniv.nl, [2]{w.j.veneman, h.p.spaink}@biology.leidenuniv.nl

1. Introduction

Biological systems evaluation can somehow reveal the mechanisms of toxicology, infectious diseases and drug targeting. Zebrafish is such a type of popular model system due to its physical transparency and genetic similarity to human beings. Zebrafish embryo can be well studied in fluorescent microscope, as there is a large amount of available fluorescent markers and genetically engineered zebrafish. Vertebrate Automated Screening Technology (VAST BioImager) has been developed [7] especially for high throughput imaging [8]. A VAST BioImager unit is used for the automated dispatching of zebrafish embryos. One-by-one the object is loaded into a tiny capillary and then put into the field of view of the imager. A full revolution of the object can be obtained by stepper motors which can rotate the specimen from any viewpoint. In Fig. 1 (a) examples of such views are depicted.

To enable the evaluation of the volume and the surface area of zebrafish, the 3D reconstruction techniques should be considered. The concept of space carving [4] is well developed in the area of computer vision – typically to reconstruct a 3D object from a range of views [3]. The VAST BioImager can generate such axial viewed images which offer prior knowledge for our purpose. The silhouettes are segmented from each individual view, which can be used for camera calibration and the visual hull construction. The proposed method can be included in a measurement pipeline that is used in all kinds of high throughput applications in the zebrafish field [1]. From the 3D reconstruction features can be derived that will contribute to the phenotyping of zebrafish.

2. 3D Carving Models Reconstruction

The proposed model [2] is depicted in Fig. 1. The almost evenly distributed axial images (84 views at most in our system) are generated and then segmented to a binary silhouette sequence which is used to calibrate the VAST BioImager camera and estimate an optimal 3D model by the space carving algorithm.

2.1. Pinhole camera model

From Figure 1 (c), the VAST BioImager imaging principle can be illustrated by the standard pinhole camera model. The mapping between a 3D world point $\mathbf{X}$ and its corresponding projective 2D point $\tilde{\mathbf{x}}$ in an image plane can be modelled as $\tilde{\mathbf{x}} = \mathbf{PX}$ (the notation of $\tilde{}$ denotes homogeneous coordinate). Basically, the camera matrix $\mathbf{P}$ can be decomposed into several components: $\mathbf{P} = \mathbf{K} \cdot \mathbf{R} \cdot [\mathbf{I} \mid -\tilde{\mathbf{C}}]$. Specifically, all the unknown configurations are parameterized as a vector $\psi = [f, k_x, k_y, u_x, u_y, \alpha, \phi, \gamma, \omega_1, ..., \omega_{n-1}]$, where n is the number of view samplings; f is the focal length; k_x and k_y are scaling factors; (u_x, u_y) is the image center; the remaining are the 3D rotation angles and translations.

2.2. 3D Carving models reconstruction

Given all the camera configurations and the axial viewed silhouettes, the original shape can be reconstructed by back-projecting all the masks to the 3D world. The final shape is actually the intersection of all projection cones. It seems like the object is gradually carved from an initial shape by a set of cone-shaped projections. Mathematically, the optimal object is acquired from the intersection of all back-projections as $\mathcal{V}^* = \bigcap_{j=1:,n} \mathcal{V}^{j*}$, where $\mathcal{V}^{j*} = \{v \mid (x^j = \mathbf{P}^j v, v \in \mathcal{V}) \cap \mathcal{S}^j \neq \varnothing\}$ means the remainder of the initial shape after each of the "projective carvings".

2.3. Camera configuration optimization

The camera matrix of $\mathbf{P}$ is generally unavailable, so the camera calibration is necessary. It can be achieved by searching the camera configuration solution space to optimize an energy function which is defined as area coherence [6], expressed as: $f(\psi) = \frac{1}{n} \sum_{j=1:n} C(\mathcal{S}^j, \mathbf{P}^j \cdot \mathcal{V})$, where the C denotes the overlap area between the silhouette and the projective image. Finally, the camera parameters optimization can be formulated as a maximization problem $\psi^* = \max_{\psi \in \Psi} f(\psi)$. The entry ψ can be assigned with a reasonable initialization. Then, the derivative-free method such as the Nelder-Mead simplex algorithm [5] can be em-

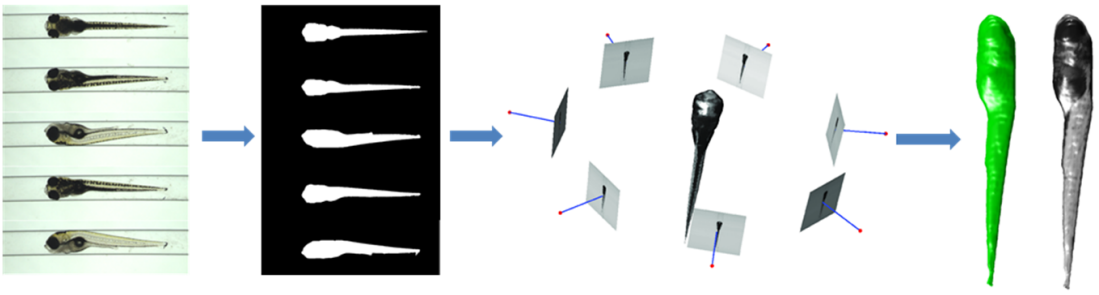

(a) (b) (c) (d)

Figure 1. 3D zebrafish model framework. (a) The original zebrafish images in different poses. (b) The corresponding silhouettes. (c) The VAST BioImager imaging scheme in a revolution. (d) The reconstructed 3D zebrafish model.

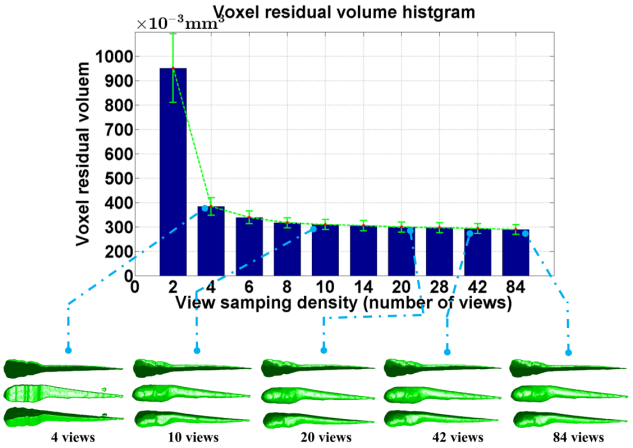

Figure 2. Experimental results

ployed to solve this problem.

3. Experiments and Discussions

A database which contains different staged zebrafish embryos is built. All zebrafish are imaged within 84 almost evenly sampled views. The figure of merit for the proposed model is shown in Fig. 2. Upper row: the voxel residual volume histgram. X direction: views sampling density (VSD). Y direction: remaining voxel volume (V_R). The views are downsampled almost uniformly from a full circulation from the original 84 views. Lower row: some selected 3D zebrafish reconstructions with different VSD. It is obvious that the larger VSD is, the more accurate reconstruction can get. One can see that with increasing VSD, the V_R decreases and asymptotically stabilises, however, a VSD larger than 20 does not produce dramatically better performance. Table 1 shows the volume and surface area measurement statistics which can be used as zebrafish evaluation references for future work. It also shows similar trend of Fig. 2 that a VSD of 20 could be the most efficient option to reconstruct an integral 3D model.

Table 1. Voxel residual (V_R) volume ($\times 10^{-3} mm^3$) and surface area (A_S) ($\times 10^{-2} mm^2$) statistics.

VSD	V_R Mean	V_R STD	A_S Mean	A_S STD
2	951.79	$\pm$140.92	1041.24	$\pm$52.98
4	383.18	$\pm$35.91	473.99	$\pm$27.74
6	338.75	$\pm$26.02	427.69	$\pm$19.91
8	316.38	$\pm$20.60	406.23	$\pm$17.94
10	309.61	$\pm$21.24	402.21	$\pm$17.94
14	305.43	$\pm$21.34	398.29	$\pm$19.00
20	298.98	$\pm$21.04	391.91	$\pm$17.05
28	296.58	$\pm$20.37	389.61	$\pm$16.40
42	293.11	$\pm$20.29	386.44	$\pm$16.39
84	289.21	$\pm$19.74	382.53	$\pm$15.69

References

[1] R. Carvalho, J. Kleijn, et al. Modeling innate immune response to early mycobacterium infection. *Computational and mathematical methods in medicine*, 2012, 2012.

[2] Y. Guo, W. Veneman, H. Spaink, and F. Verbeek. Silhouette-based 3d model for zebrafish high-throughput imaging. *IPTA'15*, 2015.

[3] C. Hernández, F. Schmitt, and R. Cipolla. Silhouette coherence for camera calibration under circular motion. *TPAMI*, 29(2):343–349, 2007.

[4] K. Kutulakos and S. Seitz. A theory of shape by space carving. *IJCV*, 38(3):199–218, 2000.

[5] J. Lagarias, J. Reeds, et al. Convergence properties of the nelder–mead simplex method in low dimensions. *SIAM Journal on optimization*, 9(1):112–147, 1998.

[6] H. Lensch, W. Heidrich, and H. Seidel. A silhouette-based algorithm for texture registration and stitching. *Graphical Models*, 63(4):245–262, 2001.

[7] C. Pardo-Martin, T. Chang, et al. High-throughput in vivo vertebrate screening. *Nature methods*, 7(8):634–636, 2010.

[8] W. Veneman, R. Marín-Juez, et al. Establishment and optimization of a high throughput setup to study staphylococcus epidermidis and mycobacterium marinum infection as a model for drug discovery. *Journal of visualized experiments*, (88), 2014.